Hindawi Publishing Corporation
EURASIP Journal on Wireless Communications and Networking
Volume 2009, Article ID 538978, 14 pages
doi:10.1155/2009/538978

*Research Article*

# Autocorrelation Properties of OFDM Timing Synchronization Waveforms Employing Pilot Subcarriers

**Oktay Üreten[1] and Selçuk Taşcıoğlu[2]**

[1] *Communications Research Centre, Terrestrial Wireless Systems Research Branch, Ottawa, ON, Canada K2H 8S2*
[2] *Electronics Engineering Department, Ankara University, 06100 Ankara, Turkey*

Correspondence should be addressed to Oktay Üreten, oktay.ureten@crc.gc.ca

Received 13 June 2008; Accepted 7 January 2009

Recommended by Marco Luise

We investigate the autocorrelation properties of timing synchronization waveforms that are generated by embedded frequency domain pilot tones in orthogonal frequency division multiplex (OFDM) systems. The waveforms are composed by summing a selected number of OFDM subcarriers such that the autocorrelation function (ACF) of the resulting time waveform has desirable sidelobe behavior. Analytical expressions for the periodic and aperiodic ACF sidelobe energy are derived. Sufficient conditions for minimum and maximum aperiodic ACF sidelobe energy for a given number of pilot tones are presented. Several useful properties of the pilot design problem, such as invariance under transformations and equivalence of complementary sets are demonstrated analytically. Pilot tone design discussion is expanded to the ACF sidelobe peak minimization problem by including various examples and simulation results obtained from a genetic search algorithm.



## 1. Introduction

Timing synchronization is an essential task of an orthogonal frequency division multiplex (OFDM) receiver, which requires alignment of the discrete Fourier transform (DFT) segments with OFDM symbol boundaries. Timing alignment errors may occur in cases where the DFT aperture contains part of the guard interval that has been distorted by intersymbol interference (ISI). This results in loss of orthogonality due to spectral leakage [1], therefore, leading to performance degradation.

Timing synchronization techniques proposed for OFDM systems can be classified as either blind or data-aided. Blind approaches exploit the inherent redundancy in the OFDM signal structure due to, for example, cyclic prefix [2] or windowing [3]. Radiometric detection and change-point estimation principles may also be employed to estimate time-of-arrival of a data frame in burst mode systems [4, 5]. Even though blind techniques have the advantage of not requiring extra overhead, their performance usually degrades when the noise level is high or the channel distortion is severe, therefore, their use is mostly limited to high signal-to-noise ratio (SNR) applications [2].

Data-aided techniques offer the advantage of superior performance in low SNR applications at the expense of reduced spectral efficiency. These techniques benefit from the correlation gain of a synchronization waveform embedded into the transmitted signal, which can be maximized by a judicious design of the waveform. In this scheme, the receiver correlates a distorted received signal with its known replica and marks the instant of maximum correlation as an estimate of the timing synchronization point. High correlation gains improve the detection of peaks buried under noise, therefore, leading to better noise immunity.

One way of embedding a synchronization waveform into a transmitted signal is to prefix it to the beginning of the time-domain waveform in the form of a preamble. Sequences with good autocorrelation properties are commonly employed in this approach. There is extensive literature on designing sequences with good autocorrelation properties; see for example [6] for an overview. Chu sequences, for instance, have perfect *periodic* autocorrelation

properties, that is, their autocorrelation values are zero except at zero lag [7]. Chu sequences belong to a class of sequences called constant amplitude zero autocorrelation (CAZAC) sequences and can be generated for arbitrary lengths. Another useful class of sequences is the generalized Barker sequences which have maximum *aperiodic* autocorrelation sidelobe amplitudes of one [8]. Unlike CAZAC sequences, there is no straightforward design scheme for generalized Barker sequences and only sequences of length up to 63 are known to date [9]. Even though, they have favorable autocorrelation properties, neither CAZAC nor Barker sequences have bandwidth restrictions. In bandlimited systems, waveforms have to be spectrally shaped to meet given bandwidth requirements to mitigate leakage to/from neighboring channels. After spectral shaping, both CAZAC and Barker sequences lose their optimal properties [10].

In addition to the time-domain embedding, synchronization waveforms can also be embedded into the transmitted signal in the frequency domain by allocating a number of subcarriers for timing in OFDM systems. In this approach, the transmitter encodes a number of pilot subcarriers with known phases and amplitudes to create a signal for timing synchronization. As the timing clock is spread over a number of discrete tones in this approach [11], synchronization can be achieved more effectively in selective fading channels [12]. Moreover, this approach facilitates the design of spectrally limited synchronization waveforms because the transmitted signal's spectral characteristics can be easily controlled by deactivating appropriate subcarriers.

In this paper, we address the autocorrelation properties of synchronization waveforms created by embedded pilot subcarriers in OFDM systems. The outline of the paper is as follows: in Section 2, the problem definition is given and our motivations are explained. A literature survey is presented and our contributions are summarized. In Section 3, background information and mathematical definitions required for derivations of the analytical expressions are given. In Section 4, sidelobe behavior of both periodic and aperiodic autocorrelation functions (ACFs) of the synchronization waveforms are investigated and analytical expressions for the sidelobe energies are derived. Some important properties of ACFs resulted from analytical expressions are introduced. In Section 5, minimization of the ACF sidelobe peak is considered as a constrained nonlinear integer programming problem and a suboptimal genetic search algorithm is utilized. In Section 6, simulation results obtained for various cases are presented. A summary and conclusions are given in Section 7. For ease of exposition most of our proofs are relegated to Appendices A, B, and C.

## 2. Preliminaries

*2.1. Problem Definition.* In this paper, we consider timing synchronization waveforms that are created by summing a number of orthogonal subcarriers called pilot tones. Merits of such synchronization waveforms depend on the selected parameters of the pilot tones such as locations, amplitudes, and phases. Although pilot design could take into account the combinations of all three parameters, in this work we narrow our focus to pilot locations only. We also assume that the number of pilots that can be allocated for synchronization is limited, that is, the number of pilot tones is less than the total number of available OFDM subcarriers. Thus, the problem addressed is manifested as the selection of the best subcarrier locations for pilot symbols such that the synchronization waveform has good autocorrelation properties. A mathematical formulation and a rigorous definition of the problem is presented in Section 4.

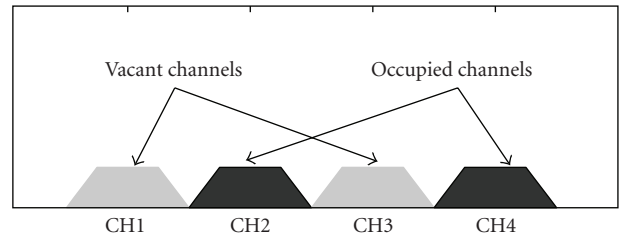


Figure 1: Timing synchronization for noncontiguous OFDM-based dynamic spectrum access poses challenges due to spectral limitation requirements, see, for example, [13, 14]. A user may decide to transmit in both vacant channels CH1 and CH3 without interfering with the user(s) in channels CH2 and CH4. More robust timing may be possible if the synchronization waveform is spread over both CH1 and CH3, which can be achieved without causing harmful interference to other user(s) by the pilot tone-based synchronization scheme investigated in this paper.

For most design problems, solutions require solving constrained nonlinear integer programming problems, for which analytical treatments are generally difficult. In this paper, we focus our attention on special cases so that we can derive analytical expressions to uncover the links between pilot placement and the autocorrelation behavior and discover some useful properties of the ACF to ease waveform design process for more complex problems.

*2.2. Motivation.* Our motive for considering the defined problem is three-fold. One reason is the overhead issue; if a design requirement can be met by using only a small number of pilot tones, then the remaining subcarriers can be used for other purposes. Although the amount of overhead savings is small in applications where the synchronization waveform is needed only in the first frame of a long packet, savings can be significant in systems that require synchronization of each OFDM frame independently, as in the ALOHA environment [12].

Our second motivation is the robustness of the reduced pilot waveforms to deviations from their design specifications. It may be possible to design a waveform with higher autocorrelation merit if all available subcarriers are utilized. However, this waveform will experience every spectral notch in the frequency-selective channel resulting in a deviation in its merit from the designed value, depending on the degree of selectivity of the channel. Although the merit of a waveform designed using a reduced number of pilots may be smaller than that of a waveform using all available

subcarriers, a reduced pilot waveform may be preferable in severely selective channels with multiple spectral notches, as it is more likely to keep its designed merit.

Our last motivation for considering the presented scheme is the increased demand for generating waveforms over fragmented (noncontiguous) frequency bands. Noncontiguous OFDM is being considered as a candidate solution for dynamic spectrum access due to its flexibility and adjustability to certain spectrum restrictions. More effective synchronization waveforms conforming to such spectral restrictions can be designed using the frequency domain pilot allocation approach, see for example the case shown in Figure 1. Therefore, the material presented in this paper can be exploited in synchronization waveform design for agile radios that are able to operate over fragmented frequency bands.

*2.3. Related Work.* Embedded frequency domain pilot subcarriers have been utilized to ease several tasks such as channel estimation [15], peak-to-average power ratio reduction [16], robust estimation of frequency offsets in frequency selective fading channels [17] and suppression of out-of-band radiation [18] in OFDM systems. Designing pilot tones for specific purposes requires judicious selection of specific parameters of the pilots such as locations, amplitudes and/or, phases. For the purpose of channel estimation, for example, the optimality condition stipulates equidistant pilots with uniform amplitudes [19, 20]. Peak-to-average power ratio reduction and sidelobe suppression problems, on the other hand, can be solved by quadratic optimization of the pilot amplitudes and phases [16, 18].

Pilot tone-assisted synchronization schemes have been adopted by wireless communications standards such as IEEE 802.11a [21] and Digital Radio Mondiale (DRM) [22]. In the IEEE 802.11a standard, uniformly spaced pilot tones modulated by a complex sequence are used to create a periodic preamble waveform to ease frame detection and timing synchronization. Periodic preambles facilitate simple autocorrelation-based metrics for timing recovery; however, a timing metric plateau inherent in these methods causes large estimation errors. In [23–25], various periodic preamble structures and metrics are proposed to improve estimation performance by creating sharper correlation peaks. In [26], performance of auto- and cross-correlation-based metrics is compared in terms of synchronization performance in an 802.11a system. The cross-correlation-based metric utilizes the long preamble for synchronization, which is created by modulating all useful subcarriers with a binary sequence. In [10], instead of using a binary sequence, the phases of all useful subcarriers are optimized through a greedy search algorithm such that the resulting time-domain waveform has good autocorrelation properties. The authors show that such synchronization waveforms outperform Barker and CAZAC sequences in a bandlimited system.

Due to reasons stressed in Section 2.2, some applications may obligate the use of a subset of all useful subcarriers. In this case, waveform design requires optimal selection of pilot tone locations as each selection results in a different autocorrelation sidelobe pattern. Such an approach is adopted in [12], in the context of an OFDM/FM system for ALOHA environment in which each OFDM frame has to be synchronized independently. Due to the limited available spectrum, only a subset of subcarriers is reserved to keep the overhead small. A suboptimal heuristic approach is used to reduce the search time of the pilot location selection process by dividing the search space into subgroups. A brute-force search is then performed in a smaller subset of subchannels and additional subchannels that provide smaller sidelobes are added into the set. In [11], a pilot tone-based synchronization scheme, inspired from a sonar waveform design approach presented in [27], is proposed for discrete multitone spread spectrum communication systems. Nonuniformly spaced pilot tones are utilized to minimize the harmonics of the autocorrelation function and reduce high sidelobe peaks by spacing pilot tones at a prime number or a Fibonacci series increment of the minimum frequency spacing. Even though the proposed selections result in better sidelobe behavior than the periodic placement, the proposed pilot configurations are far from being optimal and their use is limited due to particular spacing restrictions.

In the DRM standard [22], time reference subcarriers are allocated to perform ambiguity resolution. Locations of a predefined number of pilot cells are given in the standard; however, the design process is not disclosed. In [28], a suboptimal genetic search algorithm is proposed to yield an effective solution for the pilot tone location selection problem.

*2.4. Contributions.* Although the effect of pilot tone locations on the characteristics of the ACF has been previously noted and suboptimal search schemes have been proposed, neither a detailed investigation nor an analytical treatment of the problem has been presented in the literature.

In this paper, an in-depth discussion of pilot tone design for timing synchronization in OFDM systems is presented. Analytical expressions for both periodic and aperiodic ACF sidelobe energy are derived and sufficient conditions for obtaining minimum and maximum aperiodic ACF sidelobe energy are presented. Some useful properties of the pilot design problem such as invariance under transformations and equivalence of complementary sets are demonstrated analytically. Finally, the pilot tone design discussion is expanded by including various examples and simulation results obtained by using a genetic search algorithm.

## 3. Basic Definitions for Derivations

In this section, background information required for the derivation of analytical expressions is presented along with necessary definitions of merit measures that will be used in the following to evaluate periodic and aperiodic ACFs.

*3.1. Autocorrelation Function.* Correlation gain of a synchronization waveform is associated with its autocorrelation

characteristics. The ACF measures self-similarity of a waveform at various time lags; therefore, it is a suitable tool for estimating time of arrival of a known signal.

The ACF of a periodic discrete-time signal $s(n)$ is defined as

$$R(\tau) = \sum_{n=0}^{N-1} s(n)s^*(n+\tau), \tag{1}$$

where $\tau$ is the integer time lag and $N$ is the period of $s(n)$. $R(\tau)$ is also periodic with period $N$ and is called the periodic ACF. If $s(n)$ is not periodic, then the aperiodic ACF is employed, which is given by

$$C(\tau) = \sum_{n=0}^{N-\tau-1} s(n)s^*(n+\tau), \tag{2}$$

where $0 \le \tau \le N-1$. Here, $N$ is the length of the signal sequence which is equal to single-sided autocorrelation length.

*3.2. Merit of Autocorrelation Functions.* Merit of an ACF is associated with its sidelobe pattern, that is, the off-peak values of the correlation. A common approach to evaluate the merit of an ACF is to measure a suitable norm of its sidelobes. The $p$th-norm of the ACF sidelobe is defined as

$$L_p = \left( \sum_{\tau=1}^{N-1} |\varphi(\tau)|^p \right)^{1/p}, \tag{3}$$

where $\varphi$ can be either periodic or aperiodic ACF. The most widely used norms in merit evaluations are Euclid ($p = 2$) and Tchebychev ($p = \infty$) norms (also known as maximum norm), which are used to define sidelobe energy and sidelobe peak of the ACF as given in the following:

$$\begin{aligned} E &= L_2^2 = \sum_{\tau=1}^{N-1} |\varphi(\tau)|^2, \\ \Pi &= L_\infty = \max_{\tau \neq 0} |\varphi(\tau)| \cdot \end{aligned} \tag{4}$$

These norms are usually employed to calculate the merit factor (MF) and peak-to-side-peak ratio (PSPR); they are also defined as:

$$\begin{aligned} \mathrm{MF} &= \frac{\varphi(0)^2}{2E}, \\ \mathrm{PSPR} &= \frac{\varphi(0)}{\Pi} \cdot \end{aligned} \tag{5}$$

MF and PSPR can be combined to develop new merit measures as the minimization of one merit may not always minimize the other. Selection of which norm to consider usually depends on the specific problem; however, sidelobe energy is often employed for analytical investigations as it is more tractable than the maximum norm.

## 4. Synchronization Waveform and the Characteristics of Its ACF

Analytical treatment of pilot tone location selection problem is difficult for most cases in which the maximum norm of the ACF sidelobe is involved. In this section, we consider the Euclidian norm due to its tractability and obtain some analytical results for the ACF sidelobe energy.

*4.1. Synchronization Waveform.* An OFDM waveform is composed of a sum of orthogonal subcarriers modulated by data and/or pilot symbols. Let us assume that a subset of all subcarriers is reserved for pilot symbols to achieve robust timing synchronization and the remaining subcarriers are modulated with data. The time waveform is given by the IDFT of the modulated symbols

$$x(n) = \underbrace{\frac{1}{N} \sum_{k=1}^{N-P} a_k e^{j\Omega_k n}}_{d(n)} + \underbrace{\frac{1}{N} \sum_{k=1}^{P} b_k e^{jw_k n}}_{s(n)}, \tag{6}$$

where $\Omega_k = (2\pi/N)\alpha_k$, $w_k = (2\pi/N)\beta_k$, $\alpha_k \in S_d$, $k = 1, \ldots, N-P$, $\beta_k \in S_p$, $k = 1, \ldots, P$, and $S_d$ and $S_p$ are the data and pilot tone sets, respectively. $N$ is the DFT size, $P$ is the number of pilot subcarriers, $a_k$ and $b_k$ are the data and pilot symbols, respectively. The signals $d(n)$ and $s(n)$ are only a function of data and pilot symbols, respectively, and these waveforms are orthogonal to each other (because $S_p \cap S_d = \varnothing$) when there is no frequency offset. In the following, $s(n)$ will refer to the synchronization waveform.

Suppose that $P$ out of a total of $N$ subcarriers of an OFDM symbol are reserved for synchronization and all pilot tones are modulated by unit amplitude zero phase symbols. By fixing amplitudes and phases of the pilot symbols, we focus our attention on pilot locations only for simplicity. The corresponding time domain synchronization waveform is given by

$$s(n) = \frac{1}{N} \sum_{k=1}^{P} e^{jw_k n}. \tag{7}$$

Our objective is to select $S_p$ such that the ACF of $s(n)$ has a desirable sidelobe pattern. Both $L_2$ and $L_\infty$ norms are considered and analytical investigation of periodic and aperiodic ACF sidelobe energy is presented in subsequent sections.

*4.2. Sidelobe Energy of the Periodic ACF*

**Theorem 1** (Periodic ACF sidelobe energy theorem). *Sidelobe energy of the periodic ACF of $s(n)$ is given by*

$$\widetilde{E} = \frac{NP - P^2}{N^2} \cdot \tag{8}$$

*Proof.* See Appendix A. □

The sidelobe energy expression given in (8) can be rewritten as

$$\widetilde{E} = r(1-r), \tag{9}$$

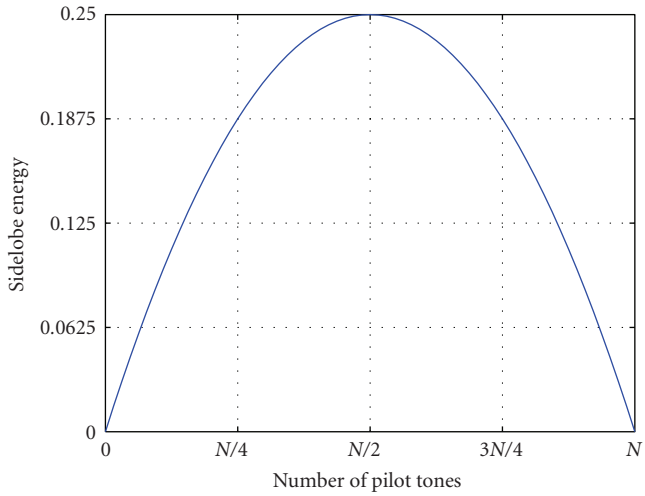


Figure 2: Relation between periodic ACF sidelobe energy and the number of pilot tones.

where $r = P/N$ is the ratio of the number of pilot tones to the total number of subcarriers. The expression (9) shows that the sidelobe energy of periodic ACF is a function of the ratio of the number of pilot tones to the total number of subcarriers only, thus it is independent of pilot tone locations.

Although the sidelobe energy expression given in (8) is derived under a zero phase assumption of the pilots, the same result holds when the pilot tones are modulated with nonzero phase symbols. This is due to the Wiener-Khinchin theorem, which relates the periodic ACF to the power spectral density via the Fourier transform. Different selections of pilot phases result in different synchronization waveforms; however, they will have a common ACF as their power spectral density functions are the same. Therefore, pilot phase selection will not improve sidelobe energy characteristics of the periodic ACF; however, proper selection of phases helps to reduce the peak-to-average-power-ratio (PAPR) of the synchronization waveform.

The relation between the number of pilot tones and the sidelobe energy of the periodic ACF is plotted in Figure 2. As seen from this figure, sidelobe energy increases with the number of pilot tones until $P = \lfloor N/2 \rfloor$ and then reduces back to zero when all subcarriers are used. However, in practice, using all subcarriers may not be possible due to bandwidth constraints. Hence, a synchronization waveform with perfect autocorrelation cannot be designed. This result is a direct consequence of the periodic ACF sidelobe energy theorem, which is formulated in (8).

*4.3. Sidelobe Energy of the Aperiodic ACF.* If a periodic correlation is employed for synchronization then at least two periods of the waveform must be embedded in the transmitted signal. If this is not feasible, due to overhead limitations, one may opt to use aperiodic, instead of periodic, correlation. In this section, aperiodic autocorrelation properties of the synchronization waveform are investigated, the aperiodic ACF sidelobe energy theorem is stated and some important corollaries resulted from this theorem are presented.

**Theorem 2** (Aperiodic ACF sidelobe energy theorem). *Sidelobe energy of the aperiodic ACF of $s(n)$ is given by*

$$\hat{E} = \frac{P}{3N} - \frac{P^2}{2N^2} + \frac{P}{6N^3} + \frac{1}{2N^3}\sum_{k=1}^{P}\sum_{l=1,\,l\neq k}^{P}\csc^2\left(\frac{w_k - w_l}{2}\right). \tag{10}$$

*Proof.* See Appendix B. □

Immediate results of this theorem follow.

**Corollary 1.** *The sidelobe energy of the aperiodic ACF depends on pilot tone locations.*

*Proof.* See (10). □

The aperiodic ACF sidelobe energy expression given in (10) can be rewritten as a sum of two terms as follows:

$$\hat{E} = \kappa + \Delta, \tag{11}$$

where

$$\kappa = \frac{P}{3N} - \frac{P^2}{2N^2} + \frac{P}{6N^3},$$
$$\Delta = \frac{1}{2N^3}\sum_{k=1}^{P}\sum_{l=1,\,l\neq k}^{P}\csc^2\left(\frac{w_k - w_l}{2}\right). \tag{12}$$

The term $\kappa$ is a function of the number of pilot tones whereas the term $\Delta$ is a function of subcarrier locations, therefore, sidelobe energy depends on the number of pilot tones as well as pilot locations.

**Corollary 2** (Invariance property). *The ACF sidelobe energy remains unchanged under any transformation of pilot set that does not change the relative distances of the pilot tones.*

*Proof.* The sidelobe energy expression given in (10) is a function of the differences of pilot locations, that is, only relative positions of the pilots determine the amount of sidelobe energy. Thus any transformation such as translations, cyclic shifts, or reversal of the pilot locations does not change the merit of the original set. □

The invariance property indicates the existence of multiple sets with identical ACF properties, which can be easily obtained by simple transformations of the original set. This property can be exploited in adaptive waveform design applications in which waveform parameters are required quickly adapt to changes in the RF environment.

The term $\Delta$ is a sum of sidelobe energy contributions due to each pilot pair. Each pilot pair contributes to the sidelobe energy with an amount depending on the separation between two pilots. A plot showing the relation between pair distance and corresponding sidelobe energy contribution is displayed in Figure 3 for $N = 64$. As seen from the figure, sidelobe energy contribution decreases with increasing pairwise pilot

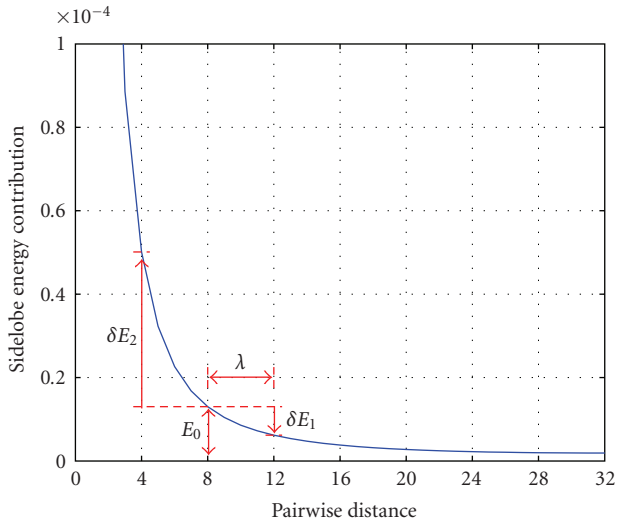


Figure 3: Relation between pairwise pilot distance and aperiodic ACF sidelobe energy contribution for $N = 64$.

distance. This observation leads to some important results of the aperiodic ACF sidelobe energy theorem, which are summarized in the following two remarks.

*Remark 1* (Maximum aperiodic ACF sidelobe energy). The sidelobe energy of the aperiodic ACF is maximum when pilot tones are placed adjacently.

As the sidelobe energy contribution of a pilot pair decreases with the pilot separation, total sidelobe energy is maximized when pilots are placed as closely as possible. This condition is satisfied when pilot tones are adjacent (no spacing between the pilots). The sidelobe energy value due to this placement is the maximum among other possible placements for the given number of pilot tones.

*Remark 2* (Minimum aperiodic ACF sidelobe energy). The sidelobe energy of the aperiodic ACF is minimum when pilot tones are placed uniformly.

As the sidelobe energy contribution of a pilot pair decreases with the pilot separation, total sidelobe energy is minimized when pilots are placed maximally spaced. This condition is satisfied when pilots are placed periodically (equal spacing between the pilots). The energy value due to this placement is the minimum possible sidelobe energy value for the given number of pilot tones.

An example is provided in Figure 4 to explain Remark 2. Assume that two pilot tones $P_1$ and $P_2$ are located at a distance of $2\Lambda$, and a third pilot $P_3$ is placed between $P_1$ and $P_2$ such that the distances from $P_1$ to $P_3$ and $P_2$ to $P_3$ are equal. We name this placement scenario the equilibrium state $E_0$, (see Figure 3). Suppose the pilot $P_3$ moves away from $P_1$ by an amount of $\lambda$, to reduce the sidelobe energy contribution of the $P_1P_3$ pair by an amount of $\delta E_1$. This movement, however, decreases the $P_2P_3$ distance, therefore, the energy contribution due to $P_2P_3$ pair increases by an

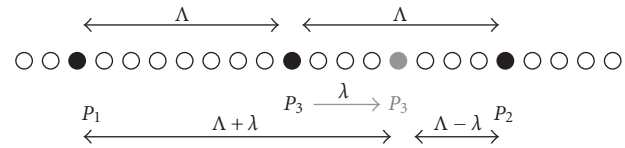


Figure 4: If a pilot moves away from one pilot, it becomes closer to another pilot in its neighborhood.

amount, $\delta E_2$. It can be shown that the sidelobe energy contribution $f(x) = \csc^2(x)$ is a convex function of the pairwise distance, therefore, $\delta E_2$ is always greater than $\delta E_1$. This requires that the sidelobe energy be higher than in the equilibrium state when the symmetry in pilot placement is broken.

In order to place all $P$ pilot tones at equal distances, $N/P$ must be an integer. Finding the minimum sidelobe energy value and the corresponding pilot placement is not straightforward if $N/P$ is not an integer. However, optimal pilot placements can be easily found for $P = N - Q$ pilots if $N/Q$ is integer. Proving this statement requires the following definition.

*Definition 1* (Complementary pilot set). For any given pilot set $S_p$ of size $P$ contained in the universal set of $S_N = 1, 2, \ldots, N$, the complementary pilot set $S_c$ of size $N - P$ is defined as the set of pilot locations not contained in $S_p$, that is $S_c = S_N - S_p$. $S_p$ and $S_c$ are called complementary sets.

**Theorem 3** (Complementary set theorem). *If $C(\tau)$ and $C'(\tau)$ are the aperiodic ACFs of the synchronization and complementary synchronization waveforms, respectively, then*

$$C'(\tau) = -C^*(N - \tau). \tag{13}$$

*Proof.* See Appendix C. □

**Corollary 3** (Equivalence of complementary sets). *The ACF sidelobe characteristics of the complementary sets are identical.*

*Proof.* The ACF sidelobe characteristics depend on the absolute value of the off-peak values of the ACF. Therefore, the proof can be shown by taking the absolute value of both the left and right sides of (13) and summing over $\tau$ values for any $P$ value:

$$\left(\sum_{\tau=1}^{N-1} \left|C'(\tau)\right|^p\right)^{1/p} = \left(\sum_{\tau=1}^{N-1} \left|C(N-\tau)\right|^p\right)^{1/p}. \tag{14}$$

□

This corollary shows how to construct a solution for a pilot set of size $N - P$ when a solution for a set size of $P$ is already available. Note that we have only shown that the sidelobe behavior of the ACFs of synchronization and complementary synchronization waveforms are identical. However, waveforms may have different energies as they are created with a different number of pilot tones; the energy differences are contained in $C(0)$ and $C'(0)$ values.

Before concluding this section, we will now introduce a trigonometric identity that is derived from the aperiodic ACF sidelobe energy expression given in (10).

**Theorem 4** (Asymptotical value of $\Delta$). .

$$\lim_{N\to\infty}\frac{1}{2N^3}\sum_{k=1}^{N}\sum_{l=1,l\neq k}^{N}\csc^2\left(\frac{\pi(k-l)}{N}\right)=\frac{1}{6}. \tag{15}$$

*Proof.* See Appendix D. □

Equation (15) shows that the sum of sidelobe energy contributions of pilot tones converges to 1/6 as the number of subcarriers approaches infinity. This series converges quite quickly; approximation error is less than $10^{-3}$ and $10^{-4}$ when $N > 16$ and $N > 40$, respectively.

*4.4. Sidelobe Peak of the ACF.* In the previous section, it was shown that equal spaced pilot placement meets the minimum ACF *sidelobe energy* requirement.

In various applications, minimization of the ACF *sidelobe peak level* may be required. A pilot sequence that minimizes ACF sidelobe energy does not necessarily guarantee a low sidelobe peak value. For example, equally spaced pilots, which can achieve the optimal sidelobe energy value, generate secondary peaks with large amplitudes, that is, grating lobes, in the ACF due to the periodicity of the waveform. When $N/P$ is integer and $P$ pilots are equally spaced, the ACF contains large peaks located at the integer multiples of $N/P$ and zeros elsewhere. The sidelobe energy is low due to the existence of a large number of zeros, however, the amplitudes of the secondary peaks become large. In this section, we consider the minimization of the sidelobe peak level.

ACF sidelobe peak level expressions for periodic and aperiodic ACFs are obtained from $|R(\tau)|$ and $|C(\tau)|$, respectively, and both can be shown to depend on pilot locations. Finding the optimal pilot locations that minimize ACF sidelobe peak level requires solving the following minimax problem:

$$S_p=\arg\min_{w_k}\max_{\tau\neq 0}|\varphi(\tau,w_k)|, \tag{16}$$

which is not tractable as the Tchebychev norm is not differentiable. This problem can be reformulated as a minimization of a differentiable $L_p$ norm where $p$ is taken as a sequence of $4, 8, 12, 16, 32, 64$. This approach (Pólya's algorithm) avoids many local minima, but unfortunately there is no guarantee that the algorithm converges to a global minimum [29].

The structure of the considered problem not only defies an analytical solution but also prevents finding nontrivial bounds for ACF sidelobe peak. The problem of obtaining lower bounds for the modulus of certain classes of trigonometrical sums has been considered in number theory and harmonic analysis literature; see for example, [30–34]. Most studies in these fields consider total or truncated sums of harmonics that are placed adjacently and they are not directly applicable to the considered synchronization waveform design problem in which the pilots are separated.

The problem of finding optimal pilot locations that minimize ACF sidelobe peak can be considered as a nonlinear integer programming problem. This is because pilot locations are only allowed to take integer values and the cost function, that is, the ACF sidelobe norm expression is nonlinear. Nonlinear integer programming problems can be efficiently solved by using suitable search techniques. In the following section, we utilize a genetic search algorithm as a viable solution for the investigation of the ACF sidelobe peak characteristics of the considered synchronization waveforms. Note that similar to other approaches such as Pólya's algorithm, the genetic algorithm (GA) used in this work does not necessarily converge to a global solution either.

## 5. Search for Lower ACF Sidelobe Peaks Using Genetic Algorithm

In this section, a brief introduction to genetic algorithms is given and basic terminology used in the genetic search literature is presented. There is an extensive literature on genetic algorithms and the interested reader is referred to [35, 36] for an in-depth discussion of the topic.

*5.1. Genetic Algorithms.* GAs are stochastic search methods inspired from the principles of biological evolution observed in nature. Evolutionary algorithms operate on a population of potential solutions by applying the principle of survival of the fittest to produce better approximations to a solution. The solution to a problem is called a chromosome. Each chromosome is made up of a collection of alleles which are the parameters to be optimized. A GA creates an initial population (a collection of chromosomes), evaluates it, then evolves the population through multiple generations in search for a good solution of a problem using the so-called genetic operators.

(i) Cross-over is a genetic operator that combines (mates) two chromosomes (parents) to produce new chromosomes (offspring).

(ii) Mutation is a genetic operator that alters one or more gene values in a chromosome from its initial state.

(iii) Selection is a genetic operator that chooses a chromosome from the current generation's population for inclusion in the next generation's mating pool. Several selection schemes can be used, such as the roulette selection rule, in which the chance of a chromosome getting selected is proportional to its fitness.

GAs have been applied to a wide variety of optimization problems including binary sequence search [37–39] and antenna array thinning [40], which bear some similarities with the pilot location selection problem considered in this paper.

*5.2. Pilot Location Search with Genetic Algorithms.* A concise description of the genetic search algorithm used for searching pilot tone locations is described in what follows. Further information regarding its convergence and its comparison to a random search can be found in [28].

An initial population of $M$ parent sequences is randomly generated. Each parent sequence is a vector of length $N$,

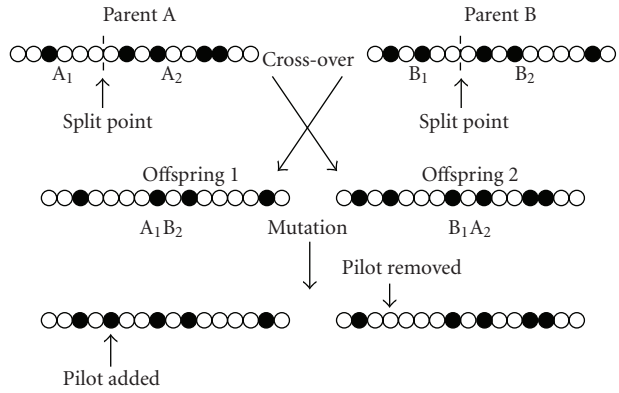


Figure 5: An illustration of cross-over and mutation operations for $P = 5$. Black circles show pilot locations.

and each element of a vector contains a binary zero or one depending on the existence of a pilot tone at that location. Time domain synchronization waveforms corresponding to the parent sequences are computed by taking the IDFT of each sequence in the population and their merits are calculated. The GA is run to minimize sidelobe peak of the aperiodic ACF.

The two sequences having the best merits (elite sequences) are kept for the next generation and then all sequences are crossed-over. The cross-over operation naturally fits to the pilot location search problem as the merit of a solution depends on the pairwise distances of pilots, which is partly preserved and diversified under the cross-over operation. At this stage, care is taken to ensure that the resulting offspring sequences have $P$ pilot tones only.

In order to prevent local minima, mutation is applied by inverting randomly selected genes. When only one bit is flipped the number of pilot tones is changed; therefore, two random bits are flipped in order to keep the pilot tone numbers fixed.

An illustration of the cross-over and mutation operations is presented in Figure 5. Chromosomes from both parents are split from a randomly chosen point and crossed-over to generate new offspring. If an offspring has more than the required pilot tones, then randomly chosen pilot(s) is/are removed. If the offspring has less pilots than required, pilot(s) is/are added randomly chosen locations.

The merits of all parent and offspring sequences are re-evaluated after each cycle. Each sequence competes for the next solution pool. The two elite sequence from the previous generation replace the worst two solutions to increase the probability of generating better sequences.

The cycle repeats a predetermined number of times or until a solution with a predefined merit is achieved.

## 6. Simulation Examples

In this section, genetic search examples are presented to gain insights into the ACF sidelobe peak behavior. In all simulations, a DFT size of $N = 64$ is used and the search algorithm runs to minimize the aperiodic ACF sidelobe peak. the initial population size is determined to be 72, as the optimal population size for problems coded as bit strings is approximately the length of the string in bits for moderate problem complexity [41]. Each member of the population is crossed-over to double the initial size of 72, then the best 72 are chosen for the next iteration.

Mutation is applied in each iteration only to the sequences that have the same merit [39]. Instead of running a single long search, multiple shorter runs are employed. In each case considered, 50 simulations starting from a different initial solution pool are run for 1000 iterations.

Three cases are investigated in the simulations. In the first example, no constraint on pilot locations is assumed; therefore, the GA explores each DFT bin as a candidate pilot location. Even though in practice some OFDM subcarriers are typically reserved for various purposes, the unconstrained case serves as a benchmark for the investigations of the ACF sidelobe peak behavior. In the second example, practical bandwidth and DC level limitations are imposed by excluding edge and zero subcarriers from the search space. In the last example, we explore the relation between pilot phases, the ACF sidelobe peak and the PAPR of synchronization waveforms.

*6.1. Unconstrained Pilot Locations.* The genetic search algorithm was run to obtain subcarrier locations for pilot set sizes of 1 to 32. Subcarrier locations for pilot set sizes of 33 to 64 can be obtained without running a search by using the complementary set theorem presented in Section 4.3.

Pilot locations extracted by the GA are shown in Figure 6. In this figure, dark circles along the vertical axis mark the locations of pilot subcarriers for a given number of pilot tones, which is shown on the horizontal axis.

Sidelobe energy values of the waveforms constructed from the pilot tone sets given in Figure 6 are shown in Figure 7. Also shown in this figure are the lower and upper sidelobe energy bounds, which can be calculated as described in Section 4.3. As seen from this figure, waveforms with low sidelobe peaks do not always have the minimal sidelobe energy, that is, minimization of sidelobe peak does not necessarily result in minimum sidelobe energy.

MF and PSPR values for the pilot sets given in Figure 6 are plotted in Figures 8 and 9, respectively. As seen from these figures, both PSPR and MF increase monotonically with the number of pilot tones when there are no constraints on pilot locations.

*6.2. Bandwidth and DC Subcarrier Restrictions.* In practical systems, transmitted waveforms must be bandlimited to meet spectral masking requirements. Such waveform bandlimiting can be accomplished in an OFDM system by deactivating the subcarriers located at the edges of the spectrum. Similarly, subcarrier zero is deactivated for receivers that cannot handle DC offsets. For the case considered in this example, the search algorithm runs in a constrained set, which excludes subcarriers $-31$ to $-27$, 27 to 31 and 0, as proposed in the IEEE 802.11a standard.

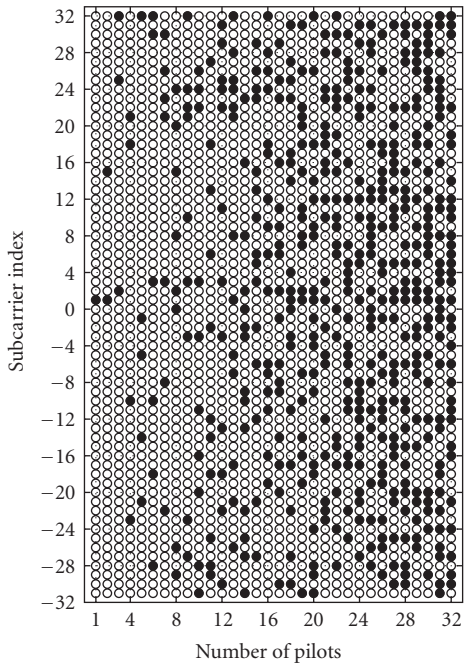


Figure 6: Pilot locations that minimize the ACF sidelobe peak for the unconstrained search. Pilot locations for $P > 32$ can be obtained directly using this figure from the complementary set theorem. For example, the configuration for $P = 40$ pilots is obtained by interchanging black and white circles of the configuration for $P = 24$ $(64 - 40 = 24)$.

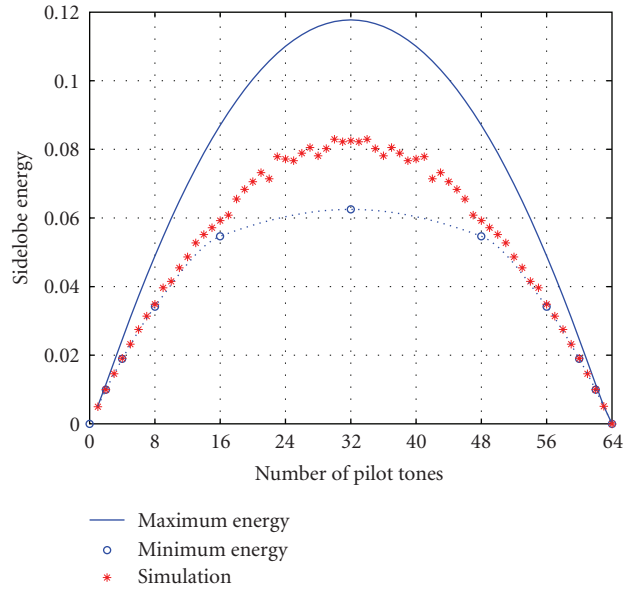


Figure 7: Aperiodic ACF sidelobe energy values of the waveforms whose sidelobe peaks are minimized. Minimum and maximum energy values are shown. (Minimum energy values for pilot numbers for which $N/P$ is not an integer are obtained by interpolation and plotted with dashed lines.)

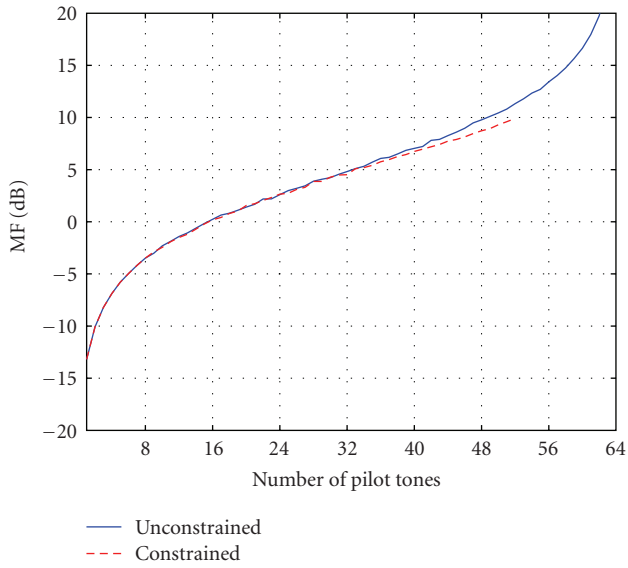


Figure 8: MF values of the synchronization waveforms.

In the constrained case, trivial solutions for $P$ values greater than $N/2$ do not exist because the complementary set theorem is not applicable due to the fact that some elements of the complementary sets will exist in the constrained region, so the GA is run for $P = 1, 2, \ldots, 52$.

Pilot locations extracted by the search algorithm are shown in Figure 10 whereas the corresponding MF and PSPR curves are plotted in Figures 8 and 9, respectively. Even though the MF of a waveform monotonically increases with the number of pilot tones, the PSPR value does not increase monotonically when there are constraints on the pilot locations. For the considered example, the maximum PSPR value is achieved when 40 out of 52 available pilots are used, and a further increase in the number of pilots degrades the PSPR.

*6.3. Nonzero Pilot Phases.* In the derivation of the analytical expressions for the aperiodic sidelobe energy in Section 4, pilot subcarriers are assumed to have zero phase to simplify analytical treatment. However, the sum of subcarriers with equal phases generates a waveform that has high PAPR, which is not desirable as it results in inefficient use of power amplifiers. The PAPR can be reduced if phase rotations are introduced on the subcarriers; however, inappropriate phase values may also increase the sidelobe peak of the ACF.

In order to explore the relations between pilot phases, the aperiodic ACF sidelobe peak and the PAPR of the synchronization waveform, PAPR and PSPR improving phases are introduced to the pilots. For PAPR reduction, we have employed Schroeder's phases [42]. These nonoptimal phases are easy to implement and are known to provide significant reduction in sidelobe peaks. For PSPR improvement, we have modified the genetic algorithm as described below to obtain proper phase values.

To generate an initial solution set, randomly drawn phase values quantized into 1024 levels are used to modulate pilot subcarriers. During the cross-over, parents swap the phases

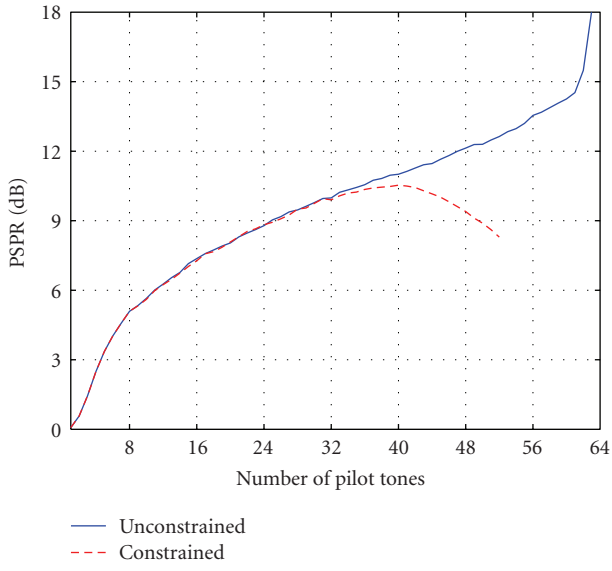


Figure 9: PSPR values of the synchronization waveforms. Note that the PSPR value does not increase monotonically with the number of pilot tones in the constrained case.

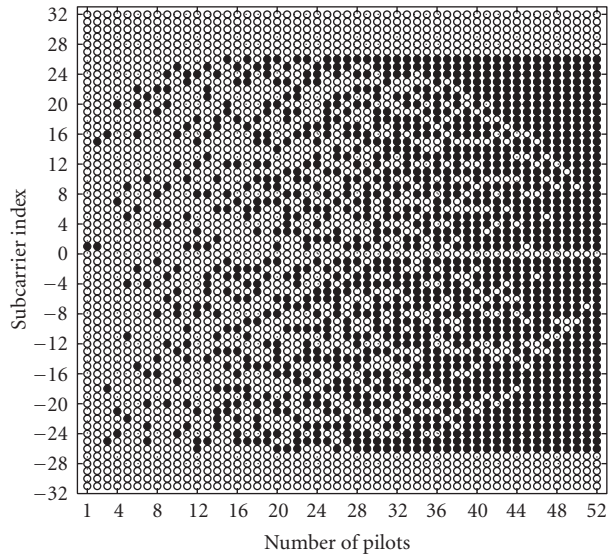


Figure 10: Pilot locations that minimize the ACF sidelobe peak for constrained search.

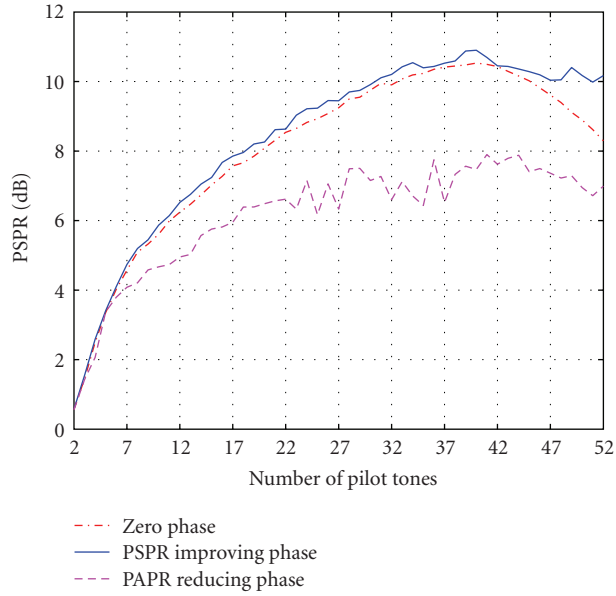


Figure 11: PSPR comparison of waveforms generated by using zero, PSPR, and PAPR reducing phases.

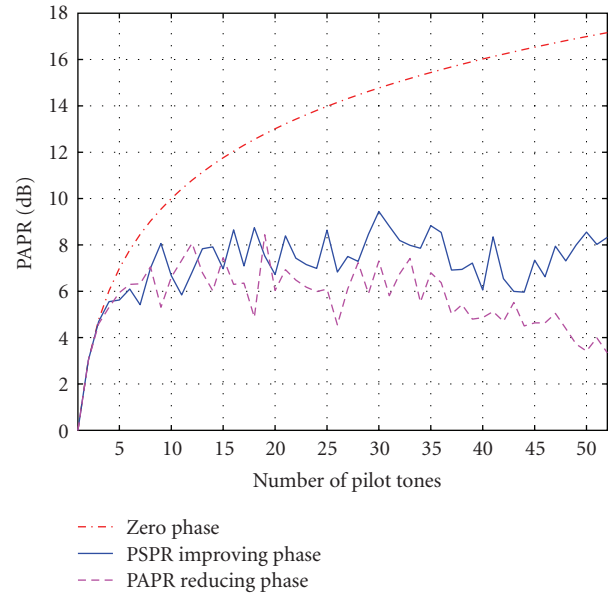


Figure 12: PAPR comparison of waveforms generated using zero, PSPR improving, and PAPR reducing phases.

of the pilots without changing their locations. Similarly, mutation is applied to the phase of a gene, which is modified with a randomly selected value from the set of quantized phase values.

PAPR reducing Schroeder's phases and PSPR improving phase values obtained from the modified GA are given in Table 1 for $P = 15$. Note that these values are the principal phase values normalized by $\pi$.

PAPR reducing Schroeder's phases and PSPR improving phase values are used to modulate pilot subcarriers. The PSPR and PAPR of the resulting waveforms are shown in Figures 11 and 12, respectively. As seen from these figures, PSPR improving phase values, which are not optimal for PAPR reduction, achieves significant PAPR reduction in addition to sidelobe peak suppression. On the other hand, even though the PAPR gain of Schroeder's phases is slightly better than the PAPR gain of the PSPR phases, Schroeder's phases degrade the PSPR significantly.

It is observed from Figure 12 that, for some $P$ values, such as $P = 12$, 15, and 19, the PAPR values of the waveforms resulting from the use of Schroeder's phases are higher than the PAPR values of the waveforms resulting from using

Table 1: Schroeder's phases ($\phi_1$) and PSPR improving phase values obtained from the modified GA ($\phi_2$) for $P = 15$.

| $k$ | $-21$ | $-20$ | $-18$ | $-15$ | $-13$ | $-10$ | $-5$ | $-3$ | $-1$ | 6 | 8 | 12 | 19 | 20 | 26 |
|---|---|---|---|---|---|---|---|---|---|---|---|---|---|---|---|
| $\phi_1$ | 1.34 | 0.88 | 1.56 | 0.06 | 1.44 | 1.03 | 0.44 | 1.06 | 0.22 | 1.72 | 0.56 | 1.59 | 0.69 | 0.91 | 1.00 |
| $\phi_2$ | 1.93 | 0.31 | 1.58 | 0.21 | 0.25 | 1.99 | 1.62 | 1.85 | 1.56 | 1.38 | 1.45 | 1.41 | 0.12 | 0.12 | 1.79 |

the GA. We note that the Schroeder's rule is a simple intuitive rule for phase angle adjustment based on the assumption that the number of harmonic components is large. Therefore, it is not implausible to observe the behavior shown in Figure 12, especially, when the number of subcarriers is small compared to the total number of subcarriers. Its simplicity paired with the fact that the Schroeder's rule may produce substantially lower peak values even when the assumption does not hold are the main motivations to use Schroeder's phases in the PAPR comparison.

## 7. Conclusions

In this paper, synchronization waveforms composed of a sum of orthogonal complex exponentials are considered for timing synchronization of OFDM systems. Sidelobe energy expressions for periodic and aperiodic ACF are derived. It is shown that the periodic ACF sidelobe energy is independent of the locations and phases of the subcarriers whereas the aperiodic ACF sidelobe energy depends on the pilot locations; therefore, optimal waveform design requires judicious selection of the pilot locations. Pilot configurations that would result in maximum and minimum sidelobe energy level for a given number of pilot tones are presented. Some properties of the ACF are introduced to use in waveform design process.

Finding pilot locations that minimize ACF sidelobe peak is not trivial; therefore, we resort to a search algorithm. Simulation results show that increasing the number of pilot tones does not necessarily improve sidelobe peak behavior of the ACF when the waveforms are spectrally constrained.

The aperiodic ACF sidelobe peak can be further reduced by proper selection of the pilot phases. When subcarrier phases are selected to further minimize the ACF sidelobe peak, the resulting waveform has a significantly reduced PAPR due to unequal pilot phases.

We have obtained the ACF sidelobe energy expressions analytically and provided pilot placement requirements for minimum and maximum aperiodic ACF sidelobe energy levels. We also considered sidelobe peak level and we employed a search algorithm for the minimization of sidelobe peak level due to the intractability of the problem. Thus, obtaining useful bounds for the aperiodic ACF sidelobe peak level remains as an open problem.

In this paper, we assumed that pilot tones are modulated by zero phase symbols in the derivation of the aperiodic ACF sidelobe energy. An analytical investigation of the impact of pilot phases on the aperiodic ACF sidelobe energy is a subject for future work.

## Appendices

## A. Proof of the Periodic ACF Sidelobe Energy Theorem (Derivation of $\widetilde{E}$)

By substituting (7) into (1) we obtain

$$\begin{aligned} R(\tau) &= \frac{1}{N^2}\sum_{n=0}^{N-1}\left(\sum_{k=1}^{P} e^{jw_k n}\right)\left(\sum_{l=1}^{P} e^{-jw_l(n+\tau)}\right) \\ &= \frac{1}{N^2}\sum_{n=0}^{N-1}\sum_{k=1}^{P}\sum_{l=1}^{P} e^{-j(w_l-w_k)n}e^{-jw_l\tau}. \end{aligned} \tag{A.1}$$

The sum terms can be split into two by grouping terms for $k = l$ and $k \neq l$ as shown in what follows:

$$R(\tau) = \frac{1}{N^2}\left[\sum_{n=0}^{N-1}\sum_{l=1}^{P} e^{-jw_l\tau} + \sum_{k=1}^{P}\sum_{l=1,\, l\neq k}^{P} e^{-jw_l\tau}\underbrace{\sum_{n=0}^{N-1} e^{-j(w_l-w_k)n}}_{\text{zero}}\right]. \tag{A.2}$$

The under braced term is equal to zero as the sum is carried over a full period of the complex exponential. Therefore, we have the following equation:

$$R(\tau) = \frac{1}{N^2}N\sum_{l=1}^{P} e^{-jw_l\tau} = \frac{1}{N}\sum_{l=1}^{P} e^{-jw_l\tau}. \tag{A.3}$$

If we substitute $R(\tau)$ in $|R(\tau)|^2 = R(\tau)R^*(\tau)$, we obtain

$$\begin{aligned} |R(\tau)|^2 &= \frac{1}{N^2}\sum_{k=1}^{P}\sum_{l=1}^{P} e^{-j(w_k-w_l)\tau} \\ &= \frac{1}{N^2}\left[P + \sum_{k=1}^{P}\sum_{l=1,\, l\neq k}^{P} e^{-j(w_k-w_l)\tau}\right]. \end{aligned} \tag{A.4}$$

Using the Euler formula, the complex exponentials on the right can be written as sums of cosine and sine terms yielding

$$|R(\tau)|^2 = \frac{1}{N^2}\left[P + \sum_{k=1}^{P}\sum_{l=1,\, l\neq k}^{P} \cos\left(w_k - w_l\right)\tau\right], \tag{A.5}$$

where we have used $\sin(-x) = -\sin(x)$.

The total sidelobe energy of the periodic ACF, $\widetilde{E}$, is given by the sum of energies of the off-peak values:

$$\widetilde{E} = \sum_{\tau=1}^{N-1} |R(\tau)|^2 \cdot \tag{A.6}$$

By substituting (A.5) into (A.6), we obtain

$$\begin{aligned}\widetilde{E} &= \frac{1}{N^2}\sum_{\tau=1}^{N-1}\left[P+\sum_{k=1}^{P}\sum_{l=1,l\neq k}^{P}\cos\left(w_k-w_l\right)\tau\right]\\ &= \frac{1}{N^2}\left[P(N-1)+\sum_{k=1}^{P}\sum_{l=1,l\neq k}^{P}\sum_{\tau=1}^{N-1}\cos\left(w_k-w_l\right)\tau\right]\\ &= \frac{1}{N^2}[P(N-1)-P(P-1)] = \frac{NP-P^2}{N^2},\end{aligned} \tag{A.7}$$

where we have used the fact that $\sum_{\tau=1}^{N-1}\cos(w_k-w_l)\tau=-1$.

## B. Proof of the Aperiodic ACF Sidelobe Energy Theorem (Derivation of $\hat{E}$)

By substituting (7) into (2) we obtain

$$\begin{aligned}C(\tau) &= \frac{1}{N^2}\sum_{n=0}^{N-\tau-1}\sum_{k=1}^{P}\sum_{l=1}^{P}e^{-j(w_l-w_k)n}e^{-jw_l\tau}\\ &= \frac{1}{N^2}\left[(N-\tau)\sum_{l=1}^{P}e^{-jw_l\tau}\right.\\ &\qquad\left.+\sum_{k=1}^{P}\sum_{l=1,l\neq k}^{P}e^{-jw_l\tau}\sum_{n=0}^{N-\tau-1}e^{-j(w_l-w_k)n}\right].\end{aligned} \tag{B.1}$$

Using geometric series expansion:

$$\sum_{n=0}^{N-\tau-1}e^{-j(w_l-w_k)n} = \frac{1-e^{j(w_l-w_k)\tau}}{1-e^{-j(w_l-w_k)}}, \tag{B.2}$$

we obtain

$$\begin{aligned}C(\tau) &= \left(1-\frac{\tau}{N}\right)R(\tau)\\ &\quad-\frac{1}{N^2}\sum_{k=1}^{P}\sum_{l=1,l\neq k}^{P}e^{-jw_l\tau}e^{j((w_l-w_k)/2)(\tau+1)}\frac{\sin((w_l-w_k)/2)\tau}{\sin((w_l-w_k)/2)}.\end{aligned} \tag{B.3}$$

Applying standard trigonometric sum formulae we obtain

$$C(\tau) = \left(1-\frac{\tau}{N}\right)R(\tau)-\frac{1}{N^2}X(\tau), \tag{B.4}$$

where

$$X(\tau) = j\sum_{k=1}^{P}\sum_{l=1,l\neq k}^{P}e^{-jw_l\tau}\cot\left(\frac{w_l-w_k}{2}\right). \tag{B.5}$$

The sidelobe energy of the aperiodic ACF is given by

$$\begin{aligned}\hat{E} &= \sum_{\tau=1}^{N-1}\left|C(\tau)\right|^2 = \sum_{\tau=1}^{N-1}C(\tau)C^*(\tau)\\ &= \sum_{\tau=1}^{N-1}\left|\left(1-\frac{\tau}{N}\right)R(\tau)\right|^2+\phi_1+\phi_2,\end{aligned} \tag{B.6}$$

where

$$\begin{aligned}\phi_1 &= -\frac{2}{N^2}\sum_{\tau=1}^{N-1}\left(1-\frac{\tau}{N}\right)\Re\{R^*(\tau)X(\tau)\},\\ \phi_2 &= \frac{1}{N^4}\sum_{\tau=1}^{N-1}\left|X(\tau)\right|^2.\end{aligned} \tag{B.7}$$

After tedious but rather straightforward calculations, one can show that $\phi_1+\phi_2=0$ by substituting $R(\tau)$ and $X(\tau)$ in (B.7) and by using the following identities [43, pages 35–37]:

$$\sum_{\tau=1}^{N-1}\sin(\tau x) = \sin\left(\frac{N}{2}x\right)\frac{\sin(((N-1)/2)x)}{\sin(x/2)}, \tag{B.8}$$

$$\sum_{\tau=1}^{N-1}\tau\,\sin(\tau x) = \frac{\sin(Nx)}{4\,\sin^2(x/2)}-\frac{N\,\cos(((2N-1)/2)x)}{2\,\sin(x/2)}. \tag{B.9}$$

Therefore, we get the following equation:

$$\begin{aligned}\hat{E} &= \sum_{\tau=1}^{N-1}\left|\left(1-\frac{\tau}{N}\right)R(\tau)\right|^2\\ &= \sum_{\tau=1}^{N-1}\left|R(\tau)\right|^2-\frac{2}{N}\sum_{\tau=1}^{N-1}\tau\left|R(\tau)\right|^2+\frac{1}{N^2}\sum_{\tau=1}^{N-1}\tau^2\left|R(\tau)\right|^2.\end{aligned} \tag{B.10}$$

The second term on the right-hand side can be shown to cancel the first term by using the following trigonometric identity [43, page 37]:

$$\sum_{\tau=1}^{N-1}\tau\,\cos(\tau x) = \frac{N\,\sin(((2N-1)/2)x)}{2\,\sin(x/2)}-\frac{1-\cos(Nx)}{4\sin^2(x/2)}. \tag{B.11}$$

The sidelobe energy of the aperiodic ACF then reduces to

$$\hat{E} = \frac{1}{N^2}\sum_{\tau=1}^{N-1}\tau^2\left|R(\tau)\right|^2. \tag{B.12}$$

This expression is calculated by substituting $|R(\tau)|^2$ given in (A.5) into (B.12). This calculation requires the sum $\sum_{\tau=1}^{N-1}\tau^2\cos(\tau x)$, which can be obtained by differentiating (B.9) with respect to $x$.

After straightforward calculations we obtain the aperiodic energy sidelobe energy expression as given in the following:

$$\hat{E} = \frac{P}{3N}-\frac{P^2}{2N^2}+\frac{P}{6N^3}+\frac{1}{2N^3}\sum_{k=1}^{P}\sum_{l=1,l\neq k}^{P}\csc^2\left(\frac{w_k-w_l}{2}\right). \tag{B.13}$$

## C. Proof of the Complementary Set Theorem

If $s(n)$ is the synchronization waveform composed using $S_p$, then the complementary synchronization waveform $s'(n)$ is given by

$$s'(n) = \frac{1}{N}\sum_{l=1}^{N-P}e^{jw_ln}. \tag{C.1}$$

Since $s(n) + s'(n) = \delta(n)$, the aperiodic ACF of the complementary synchronization waveform can be written as

$$C'(\tau) = \sum_{n=0}^{N-\tau-1} s'(n)\left[s'(n+\tau)\right]^* = \sum_{n=0}^{N-\tau-1} \left[\delta(n) - s(n)\right]\left[\delta(n+\tau) - s(n+\tau)\right]^*. \tag{C.2}$$

This reduces to

$$C'(\tau) = C(\tau) - s^*(\tau) \tag{C.3}$$

for $\tau \neq 0$. From (A.3) and (7), $R(\tau) = s^*(\tau)$. If we substitute $R(\tau)$ in (C.3) and use the well-known relation between the periodic and aperiodic ACF:

$$R(\tau) = C(\tau) + C^*(N - \tau), \tag{C.4}$$

we obtain

$$C'(\tau) = -C^*(N - \tau). \tag{C.5}$$

## D. Asymptotical Value of $\Delta$

The ACF of the synchronization waveform becomes an impulse when all subcarriers, with unit amplitude and zero phase, are used as pilots, therefore the sidelobe energy becomes zero for $P = N$. Using this observation into (10), we obtain

$$\hat{E} = 0 \Longrightarrow \Delta = \frac{1}{2} - \frac{1}{3} - \frac{1}{6N^2}. \tag{D.1}$$

Asymptotical value of $\Delta$ is then obtained in the limit case when the number of subcarriers approaches to infinity:

$$\lim_{N\to\infty} \Delta = \lim_{N\to\infty} \frac{1}{6} - \frac{1}{6N^2}. \tag{D.2}$$

Therefore, we get the following equation:

$$\lim_{N\to\infty} \frac{1}{2N^3} \sum_{k=1}^{N} \sum_{l=1, l\neq k}^{N} \csc^2\left(\frac{\pi(k-l)}{N}\right) = \frac{1}{6}. \tag{D.3}$$

## Acknowledgments

This work has been supported by Defence R&D Canada. Selçuk Taşcıoğlu was a visiting fellow at the Communications Research Centre Canada with a Grant from the International Research Fellowship Programme of the Scientific and Technological Research Council of Turkey (TÜBİTAK).

## References

[1] Y. Mostofi and D. C. Cox, "Mathematical analysis of the impact of timing synchronization errors on the performance of an OFDM system," *IEEE Transactions on Communications*, vol. 54, no. 2, pp. 226–230, 2006.

[2] J. J. van de Beek, M. Sandell, and P. O. Börjesson, "ML estimation of time and frequency offset in OFDM systems," *IEEE Transactions on Signal Processing*, vol. 45, no. 7, pp. 1800–1805, 1997.

[3] H. Bölcskei, "Blind estimation of symbol timing and carrier frequency offset in wireless OFDM systems," *IEEE Transactions on Communications*, vol. 49, no. 6, pp. 988–999, 2001.

[4] H. H. Nguyen, J. E. Salt, and Z. Zhou, "Coarse timing recovery in burst mode OFDM," in *Proceedings of the 57th IEEE Vehicular Technology Conference (VTC '03)*, vol. 1, pp. 646–650, Jeju, South Korea, April 2003.

[5] O. Üreten and N. Serinken, "Improved coarse timing for burst mode OFDM," in *Proceedings of the IEEE Global Telecommunications Conference (GLOBECOM '07)*, pp. 2841–2846, Washington, DC, USA, November 2007.

[6] P. Z. Fan and M. Darnell, *Sequence Design for Communications Applications*, John Wiley & Sons, New York, NY, USA, 1996.

[7] D. C. Chu, "Polyphase codes with good periodic correlation properties," *IEEE Transactions on Information Theory*, vol. 18, no. 4, pp. 531–532, 1972.

[8] S. W. Golomb and R. A. Scholtz, "Generalized Barker sequences," *IEEE Transactions on Information Theory*, vol. 11, no. 4, pp. 533–537, 1965.

[9] P. Borwein and R. Ferguson, "Polyphase sequences with low autocorrelation," *IEEE Transactions on Information Theory*, vol. 51, no. 4, pp. 1564–1567, 2005.

[10] G. Bumiller and L. Lampe, "Fast burst synchronization for power line communication systems," *EURASIP Journal on Advances in Signal Processing*, vol. 2007, Article ID 12145, 15 pages, 2007.

[11] M. Hirano and G. J. Veintimilla, "Non-uniformly spaced tones for synchronization waveform," US Patent no. 5896425, 1999.

[12] W. D. Warner and C. Leung, "OFDM/FM frame synchronization for mobile radio data communication," *IEEE Transactions on Vehicular Technology*, vol. 42, no. 3, pp. 302–313, 1993.

[13] J. Acharya, H. Viswanathan, and S. Venkatesan, "Timing acquisition for non contiguous OFDM based dynamic spectrum access," in *Proceedings of the 3rd IEEE International Symposium on New Frontiers in Dynamic Spectrum Access Networks (DySPAN '08)*, pp. 1–10, Chicago, Ill, USA, October 2008.

[14] K. E. Nolan, T. W. Rondeau, and L. E. Doyle, "Tests and trials of software-defined and cognitive radio in Ireland," in *Proceedings of Software Defined Radio Technical Conference and Product Exposition (SDR '07)*, Denver, Colo, USA, November 2007.

[15] S. Çöleri, M. Ergen, A. Puri, and A. Bahai, "Channel estimation techniques based on pilot arrangement in OFDM systems," *IEEE Transactions on Broadcasting*, vol. 48, no. 3, pp. 223–229, 2002.

[16] S. Hosokawa, S. Ohno, K. Teo, and T. Hinamoto, "Pilot tone design for peak-to-average power ratio reduction in OFDM," in *Proceedings of the IEEE International Symposium on Circuits and Systems (ISCAS '05)*, pp. 6014–6017, Kobe, Japan, May 2005.

[17] A. F. Kurpiers and V. Fischer, "Open-source implementation of a Digital Radio Mondiale (DRM) receiver," in *Proceedings of the 9th International Conference on HF Radio Systems and Techniques*, pp. 86–90, Bath, UK, June 2003.

[18] S. Brandes, I. Cosovic, and M. Schnell, "Sidelobe suppression in OFDM systems by insertion of cancellation carriers," in *Proceedings of the 62nd IEEE Vehicular Technology Conference (VTC '05)*, vol. 1, pp. 152–156, Dallas, Tex, USA, September 2005.

[19] M. Dong and L. Tong, "Optimal design and placement of pilot symbols for channel estimation," *IEEE Transactions on Signal Processing*, vol. 50, no. 12, pp. 3055–3069, 2002.

[20] S. Song and A. C. Singer, "Pilot-aided OFDM channel estimation in the presence of the guard band," *IEEE Transactions on Communications*, vol. 55, no. 8, pp. 1459–1465, 2007.

[21] IEEE Std. 802.11a-1999, "Part 11: Wireless LAN Medium Access Control (MAC) and Physical Layer (PHY) Specifications: High-speed Physical Layer in the 5 GHz Band," 1999.

[22] European Telecommunications Standards Institute (ETSI), "ES 201 980, Digital Radio Mondiale (DRM)," 2004.

[23] H. Minn, M. Zeng, and V. K. Bhargava, "On timing offset estimation for OFDM systems," *IEEE Communications Letters*, vol. 4, no. 7, pp. 242–244, 2000.

[24] B. Park, H. Cheon, C. Kang, and D. Hong, "A novel timing estimation method for OFDM systems," *IEEE Communications Letters*, vol. 7, no. 5, pp. 239–241, 2003.

[25] K. Shi and E. Serpedin, "Coarse frame and carrier synchronization of OFDM systems: a new metric and comparison," *IEEE Transactions on Wireless Communications*, vol. 3, no. 4, pp. 1271–1284, 2004.

[26] A. Fort, J.-W. Weijers, V. Derudder, W. Eberle, and A. Bourdoux, "A performance and complexity comparison of autocorrelation and cross-correlation for OFDM burst synchronization," in *Proceedings of IEEE International Conference on Acoustics, Speech, and Signal Processing (ICASSP '00)*, pp. 341–344, Istanbul, Turkey, June 2000.

[27] H. Cox and H. Lai, "Geometric comb waveforms for reverberation suppression," in *Proceedings of the 28th Asilomar Conference on Signals, Systems and Computers (ACSSC '94)*, vol. 2, pp. 1185–1189, Pacific Grove, Calif, USA, October-November 1994.

[28] O. Üreten, S. Taşcıoğlu, N. Serinken, and M. Yılmaz, "Search for OFDM synchronization waveforms with good aperiodic autocorrelations," in *Proceedings of IEEE Canadian Conference on Electrical and Computer Engineering (CCECE '04)*, vol. 1, pp. 13–18, Niagara Falls, Canada, May 2004.

[29] P. Guillaume, J. Schoukens, R. Pintelon, and I. Kollar, "Crest-factor minimization using nonlinear Chebyshev approximation methods," *IEEE Transactions on Instrumentation and Measurement*, vol. 40, no. 6, pp. 982–989, 1991.

[30] L. Carlitz and S. Uchiyama, "Bounds for exponential sums," *Duke Mathematical Journal*, vol. 24, no. 1, pp. 37–41, 1957.

[31] D. R. Anderson and J. J. Stiffler, "Lower bounds for the maximum moduli of certain classes of trigonometric sums," *Duke Mathematical Journal*, vol. 30, no. 1, pp. 171–176, 1963.

[32] S. V. Konyagin and M. A. Skopina, "Comparison of the $> L^1$-norms of total and truncated exponential sums," *Mathematical Notes*, vol. 69, no. 5-6, pp. 644–651, 2001.

[33] P. Oswald, "Extremal properties of trigonometric polynomials with applications to signal design," in *Proceedings of International Conference on Trends in Approximation Theory*, pp. 343–352, Nashville, Tenn, USA, October 2001.

[34] E. Belinsky, "Some extremal problems for trigonometric polynomials," *Journal of Mathematical Analysis and Applications*, vol. 286, no. 2, pp. 675–681, 2003.

[35] J. H. Holland, *Adaptation in Natural and Artificial Systems*, MIT Press, Cambridge, Mass, USA, 1992.

[36] D. E. Goldberg, *Genetic Algorithms in Search, Optimization and Machine Learning*, Addison-Wesley Longman, Boston, Mass, USA, 1989.

[37] B. Militzer, M. Zamparelli, and D. Beule, "Evolutionary search for low autocorrelated binary sequences," *IEEE Transactions on Evolutionary Computation*, vol. 2, no. 1, pp. 34–39, 1998.

[38] X. Deng and P. Fan, "New binary sequences with good aperiodic autocorrelations obtained by evolutionary algorithm," *IEEE Communications Letters*, vol. 3, no. 10, pp. 288–290, 1999.

[39] S. E. Kocabas and A. Atalar, "Binary sequences with low aperiodic autocorrelation for synchronization purposes," *IEEE Communications Letters*, vol. 7, no. 1, pp. 36–38, 2003.

[40] R. L. Haupt, "Thinned arrays using genetic algorithms," *IEEE Transactions on Antennas and Propagation*, vol. 42, no. 7, pp. 993–999, 1994.

[41] J. T. Alander, "On optimal population size of genetic algorithms," in *Proceedings of Computer Systems and Software Engineering (CompEuro '92)*, pp. 65–70, The Hague, The Netherlands, May 1992.

[42] M. Schroeder, "Synthesis of low-peak-factor signals and binary sequences with low autocorrelation," *IEEE Transactions on Information Theory*, vol. 16, no. 1, pp. 85–89, 1970.

[43] I. S. Gradshtein and I. M. Ryzhik, *Table of Integrals, Series, and Products*, Academic Press, San Diego, Calif, USA, 2000.